Mode selection and tuning of single-frequency short-cavity VECSELs

Darwin Serkland, Haley So, Gregory Peake, Michael Wood, Alejandro Grine, et al.

Darwin K. Serkland, Haley M. So, Gregory M. Peake, Michael G. Wood, Alejandro J. Grine, Christopher P. Hains, Kent M. Geib, Gordon A. Keeler, "Mode selection and tuning of single-frequency short-cavity VECSELs," Proc. SPIE 10552, Vertical-Cavity Surface-Emitting Lasers XXII, 1055206 (5 March 2018); doi: 10.1117/12.2291197

SPIE.

Event: SPIE OPTO, 2018, San Francisco, California, United States

Mode selection and tuning of single-frequency short-cavity VECSELs

Darwin K. Serkland*, Haley M. So†, Gregory M. Peake, Michael G. Wood,
Alejandro J. Grine, Christopher P. Hains, Kent M. Geib, Gordon A. Keeler‡
Sandia National Laboratories, Albuquerque, NM 87185

ABSTRACT

We report on mode selection and tuning properties of vertical-external-cavity surface-emitting lasers (VECSELs) containing coupled semiconductor and external cavities of total length less than 1 mm. Our goal is to create narrow-linewidth (<1MHz) single-frequency VECSELs that operate near 850 nm on a single longitudinal cavity resonance and tune versus temperature without mode hops. We have designed, fabricated, and measured VECSELs with external-cavity lengths ranging from 25 to 800 μm. We compare simulated and measured coupled-cavity mode frequencies and discuss criteria for single mode selection.

Keywords: VCSEL, tunable laser, mode selection, linewidth, frequency noise, atomic clocks, spectroscopy

1. INTRODUCTION

Recently, single-mode 50-MHz-linewidth vertical-cavity surface-emitting lasers (VCSELs) have enabled 1ow-power (less than 125 mW) chip-scale atomic clocks (CSACs) that rely on spectroscopic interrogation of alkali atoms, typically rubidium or cesium.[1-2] A VCSEL with a linewidth less than 1 MHz is needed for next-generation low-power atomic clocks to achieve performance approaching that of primary frequency standards, such as atomic beam and fountain clocks.[3] Two wavelengths of interest for such narrow-linewidth VCSELs are 780 nm (for rubidium) and 852 nm (for cesium). To be useful, the VCSEL must also be tunable to the precise atomic resonance wavelength.

The Schawlow-Townes laser linewidth formula[4] shows a clear path to reduce the VCSEL linewidth by orders of magnitude: namely, increase the photon lifetime in the cavity. Fundamentally, laser linewidth is due to frequency fluctuations that occur when a photon is spontaneously emitted into the laser mode, adding one quantum of electric field at a random phase angle to the existing laser field. The laser linewidth due to spontaneous emission is given by the modified Schawlow-Townes linewidth formula

$$\Delta\nu_{ST} = \left(h\nu/P_0\right)\left(\pi n_{sp}\eta_0\right)\left(\Delta\nu_C\right)^2, \tag{1}$$

where $\Delta\nu_C$ (≈80 GHz) is the linewidth of the cold cavity (*i.e.*, without active region gain or loss), $h\nu$ (≈1.5 eV) is the photon energy, P_0 (≈1 mW) is the output power, n_{sp} (≈2) is the population inversion factor, and η_0 (≈0.5) is the optical output coupling efficiency. In 1982, Henry explained the observations of much larger linewidths of semiconductor lasers by the formula

$$\Delta\nu = \Delta\nu_{ST}\left(1+\alpha^2\right), \tag{2}$$

where α (≈3) is the linewidth enhancement factor of the active region material, which accounts for the fact that carrier density fluctuations in the semiconductor cause refractive index fluctuations that perturb the laser frequency.[5] For a conventional VCSEL structure, a typical lasing linewidth is $\Delta\nu$ = 50 MHz, calculated using the typical parameter values shown in parentheses above.

A few clear strategies to reduce VCSEL linewidth are suggested by equations (1) and (2): increase single-mode output power, decrease cold-cavity linewidth (either by increasing cavity length or decreasing round-trip optical losses), and reduce the linewidth enhancement factor. In order to achieve a 50-fold reduction in VCSEL linewidth, from 50 to 1 MHz, we choose to decrease the cold-cavity linewidth $\Delta\nu_C$ by a factor of 7. The linewidth of a cold cavity follows the

* DKSERKL@sandia.gov; phone: (505) 844-5355; http://www.sandia.gov/
† Current affiliation: Columbia University, New York, NY 10027.
‡ Current affiliation: Defense Advanced Research Projects Agency, Arlington, VA 22203.

Vertical-Cavity Surface-Emitting Lasers XXII, edited by Chun Lei, Kent D. Choquette, Proc. of SPIE
Vol. 10552, 1055206 · © 2018 SPIE · CCC code: 0277-786X/18/$18 · doi: 10.1117/12.2291197

equation $\Delta\nu_c = cT/(n_c 2L_c)$, where c is the speed of light, T is the round-trip power transmission loss, n_c is the index of the cavity, and L_c is the effective length of the cavity. Hence, increasing the effective length of a VCSEL cavity, by using an external-cavity mirror, will decrease the cold-cavity linewidth.

Figure 1(a) shows a schematic drawing of a vertical-external-cavity surface-emitting laser (VECSEL) containing two coupled cavities: a short semiconductor cavity and a longer external cavity, of length less than 1 mm. We have designed, fabricated, and measured VECSELs with external cavity lengths ranging from 25 to 800 μm. Semiconductor epitaxial layers form the bottom high-reflecting distributed Bragg reflector (DBR), the quantum well optical gain region, and a partially reflecting middle DBR. The external cavity is made of air or glass and an external dielectric output-coupling DBR. For size reference, we show in Figure 1(b) a schematic drawing of a standard VCSEL containing just two semiconductor DBRs: bottom and top. While the total thickness of the VCSEL epitaxial layers is about 8 μm, the effective cavity length is only about 1 μm.

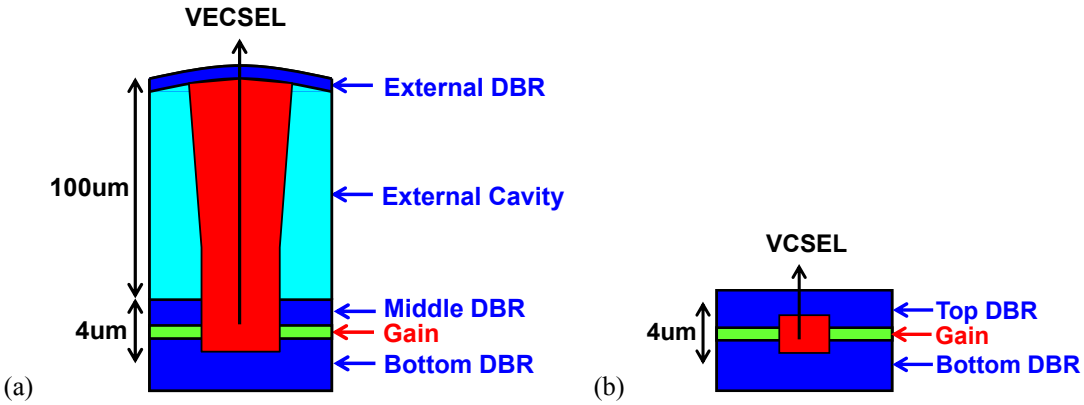

Figure 1. (a) Schematic drawing of a coupled-cavity VECSEL having a "middle mirror" between the short semiconductor cavity and the longer external cavity. (b) Schematic drawing of a standard 2-mirror VCSEL cavity, showing a much shorter cavity length. The effective cavity length of a VCSEL with a 1-wave active region is about 4 wavelengths in the material, or about 1 μm.

In the following sections, we will consider a specific VECSEL design that we have fabricated, tested, and modeled. This VECSEL design employs a 36-period semiconductor bottom DBR, a 1-wave cavity layer containing the optical gain region, a 4-period semiconductor middle DBR, a 30.25-wave air external cavity, and an 8-period dielectric (SiO_2/SiN) external DBR.

2. COUPLED-CAVITY THEORY AND MODELING

In this section, we will consider the theory and modeling of longitudinal modes in a VECSEL cavity similar to that shown in Figure 1(a). In particular, we seek a theoretical understanding of external-cavity designs that achieve (1) single-mode oscillation, (2) narrow linewidth, and (3) mode-hop-free tuning versus temperature. We start by considering a simplified three-mirror model of the coupled-cavity VECSEL, shown in Figure 2(a). The VECSEL contains two sections: a semiconductor section of length L_s that contains the optical gain medium, and a passive external-cavity section of length L_p. We can obtain analytical equations if we temporarily treat the three mirrors as infinitely thin with real and positive field reflection coefficients r_1, r_2, and r_3, as drawn in Figure 2(a). The three-mirror VECSEL model of Figure 2(a) can be reduced to an equivalent two-mirror cavity model, shown in Figure 2(b), by replacing the external-cavity section with an equivalent single mirror of effective (complex) field reflection coefficient r_{eff}. The external-cavity section, shown in Figure 2(a), acts as a Fabry-Perot cavity of length L_p, and has a complex field reflection coefficient r_{eff} that depends on wavelength according to the equation

$$r_{eff} = r_0 \exp(i\phi_e) = \frac{r_3 \exp(i\phi_p) - r_2}{1 - r_2 r_3 \exp(i\phi_p)}, \tag{3}$$

where $\phi_p = 2k_p L_p$ is the round-trip phase shift in the external cavity, $k_p = 2\pi n_p/\lambda_0$ is the k-vector in the external cavity, n_p is the index of refraction in the external cavity, and λ_0 is the wavelength (in vacuum).

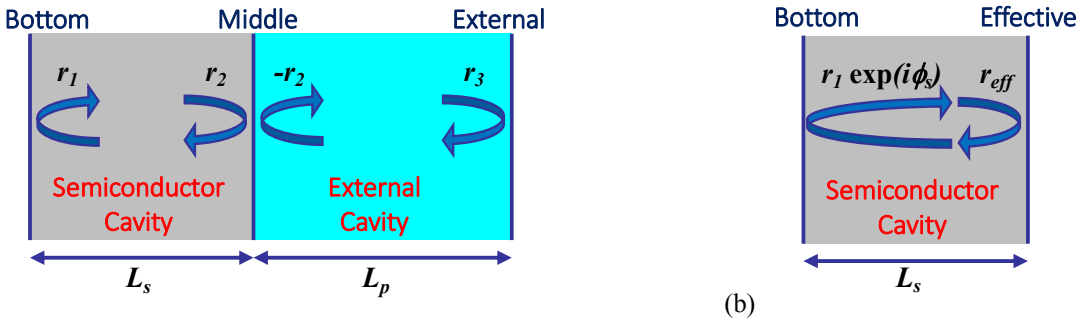

Figure 2. Simplified model of a three-mirror external-cavity laser, showing infinitely thin mirrors with real (and positive) field reflection coefficients r_1, r_2, r_3. (a) Three-mirror laser cavity showing a semiconductor section of length L_s and a passive external-cavity section of length L_p. (b) Equivalent two-mirror laser cavity obtained by replacing the external cavity section with a single effective mirror of complex field reflection coefficient r_{eff}.

In Figure 3(a), we plot the amplitude r_0 and the phase ϕ_e of the complex reflection coefficient r_{eff}, for an external cavity length of 25.7125 μm (30.25 wavelengths at 850 nm), bounded by a middle mirror with field reflection $r_2 = 0.8376$ and an external mirror with field reflection $r_3 = 0.9916$. We note that the external cavity length L_p was chosen to create a Fabry-Perot anti-resonance at the intended laser wavelength of 850 nm, causing the field reflection coefficients r_2 and r_3 to add constructively to yield a larger effective reflection coefficient $r_0 = 0.9985$ and a phase shift of 0 degrees at 850 nm. Hence, for a semiconductor length L_s equal to an integer number of half wavelengths, we expect a low-loss cavity resonance at 850 nm, since the effective mirror reflection r_{eff} (very near 850 nm) approximates that of a typical top distributed Bragg reflector (DBR) in a standard VCSEL cavity. The effective reflection coefficient r_{eff} of the compound mirror exhibits minima at external-cavity resonances, such as at λ_{R1}=829.95, λ_{R2}=843.2, λ_{R3}=856.9, and λ_{R4}=871.05 nm, indicating a free-spectral range (FSR) of 13.7 nm at 850 nm. Figure 3(a) shows numerical (transmission matrix) simulations of the actual VECSEL DBRs (a 4-period middle DBR and an 8-period external DBR), although the Fabry-Perot equation (3) would yield similar results from 830 to 870 nm. In the simulations, we assumed semiconductor DBRs with high index 3.51 and low index 3.03, and a dielectric DBR with high index 1.96 and low index 1.46.

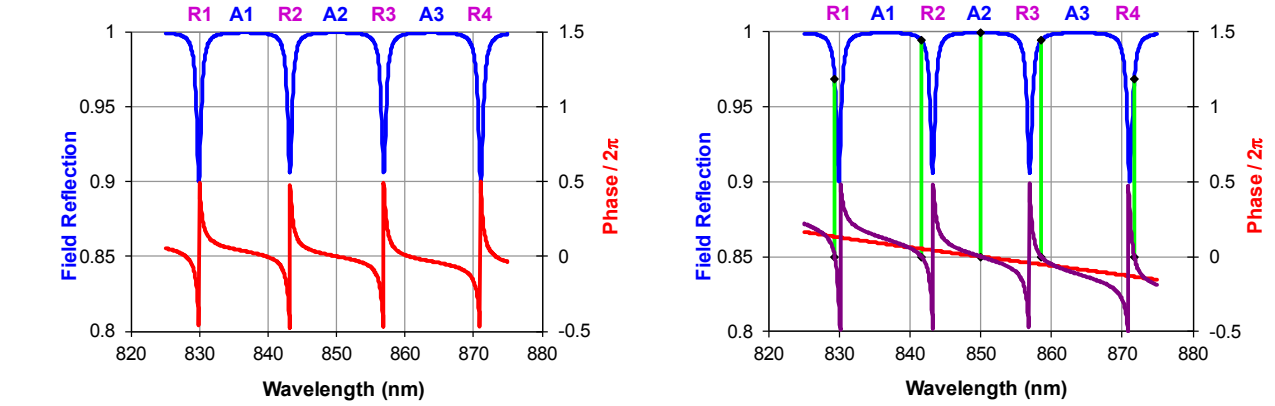

Figure 3. (a) Amplitude and phase of the effective reflection coefficient r_{eff}, for $r_2 = 0.8376$ (4-period semiconductor DBR terminated by air), $r_3 = 0.9916$ (8-period SiO2/SiN DBR terminated by air on both sides), and $L_p = 25.7125$ μm. The external cavity length was chosen as 30.25 wavelengths to create an anti-resonance (A2) at 850 nm. External-cavity resonances are denoted by R1, R2, R3, R4, and anti-resonances are denoted by A1, A2, A3. (b) The round-trip phase shift (red) versus wavelength in the 1-wavelength semiconductor cavity of length $L_s = 242$ nm. The round-trip VECSEL phase shift (purple) on the right side of equation (4), obtained by adding the phase shifts from r_{eff} and the semiconductor cavity. VECSEL cavity resonances occur when the round-trip phase shift (purple) is an integer multiple of 2π, and the vertical green lines show the amplitude of r_{eff} at these resonance wavelengths.

In order to achieve laser threshold, the semiconductor section must provide sufficient round-trip gain and phase shift that the electric field exactly reproduces itself after one round-trip in the laser cavity. The effect of optical gain in the semiconductor section is to multiply the electric field by a round-trip gain coefficient γ=exp(gL), where gL is the one-way power gain in the semiconductor region. Hence, we can write the laser threshold equation as

$$1 = r_{eff}\,\gamma\; r_1 \exp(i\phi_s)\,, \tag{4}$$

where $\phi_s = 2k_sL_s$ is the round-trip phase shift in the semiconductor cavity, $k_s = 2\pi n_s/\lambda_0$ is the k-vector in the semiconductor cavity, n_s is the index of refraction in the semiconductor cavity, and λ_0 is the wavelength (in vacuum).

Only a discrete set of wavelengths (cavity resonance wavelengths) satisfy equation (4). In particular, resonances occur when the phase of the complex number on the right side of equation (4) equals an integer multiple of 2π. In Figure 3(b), we plot the phase (red) of the complex reflection coefficient $r_1 \exp(i\phi_s)$, for a 36-period bottom DBR and a 1-wave semiconductor section of length L_s = 242 nm = λ_0 / n_s. The purple curve in Figure 3(b) is the round-trip VECSEL cavity phase shift, which is the sum of the phase shifts from r_{eff} and $r_1 \exp(i\phi_s)$. The vertical green lines intersect the graph of the effective reflection r_{eff} at the VECSEL cavity resonant wavelengths (i.e., at zero crossings of the net phase shift).

Given that the single-pass power gain gL is a small number, we make the approximation $1/\gamma$=exp(-gL)=1-gL in equation (4) to obtain an equation for the threshold power gain gL

$$gL = 1 - r_{eff}\, r_1 \exp(i\phi_s). \tag{5}$$

Equation (5) can be considered as two equations: one equation for amplitude and a second equation for phase. Figure 4(a) shows a plot of the magnitude of the right-hand side of equation (5) versus wavelength (blue) and the round-trip phase shift versus wavelength (purple). At the cavity resonance wavelengths that satisfy the round-trip phase condition, equation (5) becomes real and yields a minimum value for the threshold gain gL. In Figure 4(a), five narrow local minima appear at wavelengths that satisfy the round-trip phase condition, and the magnitude of gL at these minima is the one-way threshold power gain of the corresponding laser modes. The table in Figure 4(b) lists the coupled-cavity resonance wavelengths and the corresponding threshold power gain values gL. Single-mode lasing at 850 nm occurs because the 850-nm mode has a far lower threshold gain value than the other longitudinal cavity modes.

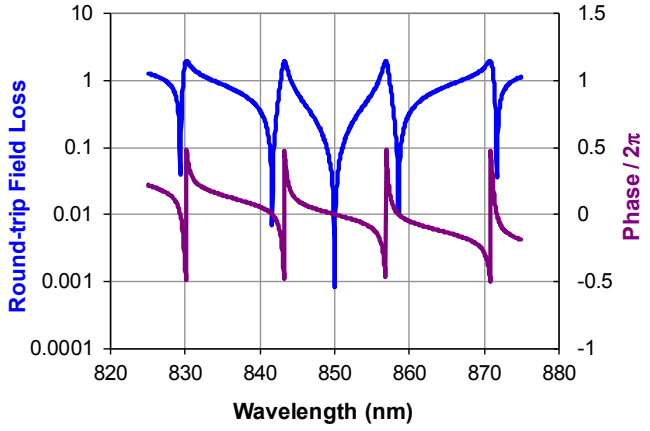

(a)

(b)

Mode Wavelength (nm)	Threshold Gain	Relative Threshold Gain
829.35	0.0384	47.1
841.65	0.0067	8.3
850.00	0.0008	1.0
858.50	0.0107	13.1
871.70	0.0358	44.0

Figure 4. (a) Round-trip field loss versus wavelength. The plot shows the magnitude of the complex number on the right-side of equation (5) versus wavelength (blue). Minima occur when the round-trip phase shift (purple) is a multiple of 2π, and correspond to longitudinal cavity modes. (b) Mode wavelengths and their corresponding threshold gain values. Threshold gain increases off resonance and thus threshold accuracy is limited by the 0.05 nm wavelength resolution of this simulation, and since we expect symmetric results around the 850-nm mode, the lowest gain values within each pair of symmetric modes (0.0067 and 0.0358) are the most accurate.

Next we consider the electric-field profile and cold-cavity linewidth for two particular modes of the VECSEL cavity discussed above. We use transmission matrix calculations[6] to model the VECSEL cavity having the refractive index profile versus position shown in Figure 5(a) and 5(b). The semiconductor DBRs are modeled as containing pairs of high

index n_{16} = 3.51 and low index n_{92} = 3.03 quarter-wavelength-thick layers at 850 nm, corresponding to $Al_xGa_{1-x}As$ with x=0.16 and 0.92, respectively. The bottom semiconductor DBR contains 36 periods, yielding a power reflectivity of 0.9999. The semiconductor cavity length is L_s = 242.2 nm, which is 1 wavelength of thickness in the semiconductor material of index 3.51. Due to field penetration into the DBR layers, the effective semiconductor cavity length is approximately 4 waves rather than the 1-wave physical length. The external cavity length is taken to be 25.7125 μm of air, or 30.25 waves at 850 nm. The external mirror is a dielectric DBR consisting of 8 pairs of SiO2 (n = 1.46) and Si_3N_4 (n = 1.96). In order to phase match the dielectric DBR to air on both sides, the quarter-wave SiO2 layer in the first period is replaced by a quarter-wave layer of air. This VECSEL design is similar to the one we reported previously.[7] Figure 5(a) shows the resulting optical intensity (electrical field modulus squared) of the 850-nm mode versus distance z from the GaAs substrate. Figure 5(b) shows a zoomed-in view of the semiconductor-to-air interface at z = 5.5 μm, which clearly shows that the optical intensity peaks in the 1-wave semiconductor active region. The optical intensity decays within the 4-period middle DBR to a lower-intensity standing wave in the air external cavity section.

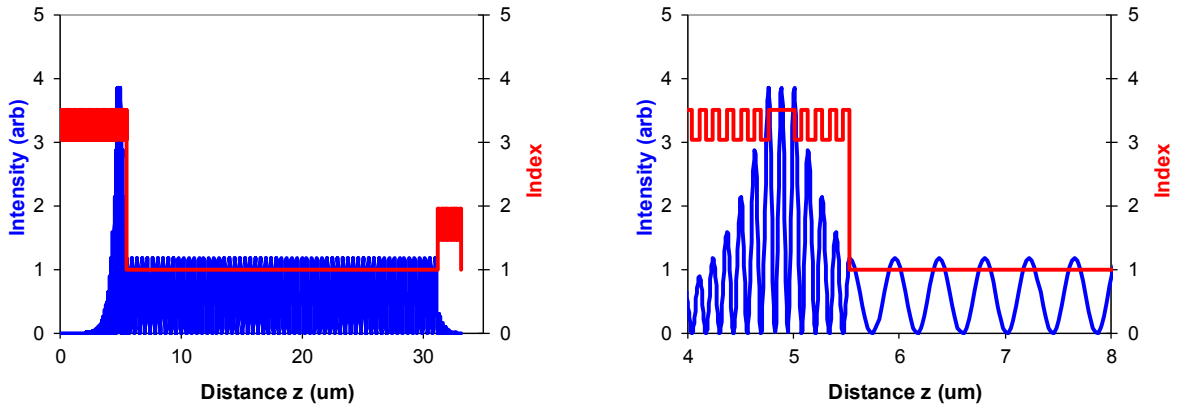

(a) (b)

Figure 5. (a) Optical intensity (blue) at 850 nm and index of refraction (red) versus position in the VECSEL cavity. (b) Zoomed view of the optical intensity at 850 nm and index of refraction at positions from 4 to 8 μm from the bottom of the semiconductor DBR. The 1-wave cavity appears near z = 5 um and the middle 4-period DBR appears between z = 5.1 and 5.5 um.

Figure 6 shows the reflection spectrum of the VECSEL cavity, as viewed from outside the external-cavity mirror. We have zoomed in on the three modes nearest to 850 nm (841.65 , 850, and 858.55 nm). The 850-nm mode operates on a resonance of the semiconductor cavity and an anti-resonance of the external cavity, and has very low round-trip losses that yield a low threshold current. For these simulations, the 1-wavelength-long (242.2 nm) active cavity layer is assumed to have a uniform power loss coefficient of 3 cm^{-1}, which yields a one-way power loss of 7.27 x 10^{-5} for propagation through the 1-wave cavity layer. This loss is approximately 10 times smaller than the threshold gain that is required to compensate for output coupling transmission losses through the top of the external cavity as given in Figure 4(b). Hence, the simulated cold-cavity linewidth of 0.0184 nm (7.6 GHz), visible in Figure 6(b), is dominated by output coupling transmission losses from the VECSEL cavity. The narrow cold-cavity linewidth of the 850-nm mode results in a measured VECSEL linewidth of 2 MHz as will be discussed below.

Figure 7(a) shows the optical intensity versus position of the λ_1 = 841.642 nm mode. Also shown in Figure 7(a) is the index of refraction versus position, which shows that the optical intensity is highest in the external cavity section. The high optical intensity in the external cavity is consistent with the fact that this mode operates close to the 843.2-nm resonance wavelength of the external cavity. Because the effective reflectivity r_e of the external cavity is only 0.99 at 841.642 nm, the threshold of this mode is approximately 8 times higher than that of the 850 nm mode. Hence, the 841.642 nm mode is unlikely to ever achieve threshold. Figure 7(b) shows a zoomed view of the reflectivity versus wavelength that resolves the 0.032 nm cold-cavity linewidth of the 841.642 nm mode.

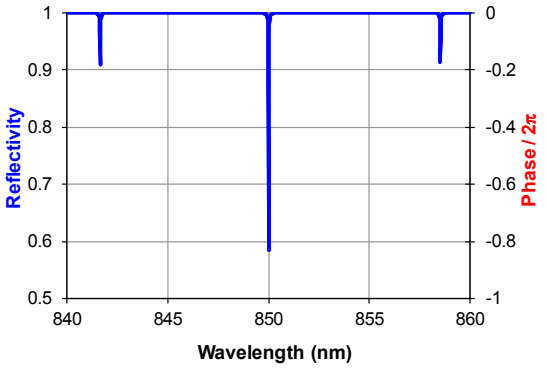

(a)

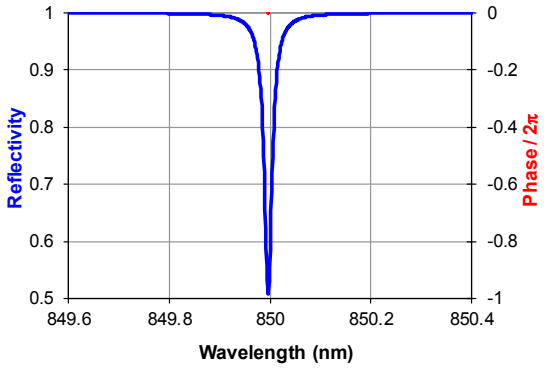

(b)

Figure 6. (a) VECSEL reflectivity versus wavelength, showing the three modes closest to 850 nm. The mode at 850 nm operates on an anti-resonance of the external cavity. The adjacent modes, at 841.64 and 858.52 nm, operate approximately 1.6 nm from external-cavity resonance wavelengths shown in Figure 3(b) above. (b) Zoomed view of the 850 nm resonance dip showing a full width at half maximum (FWHM) of 0.0184 nm (7.6 GHz).

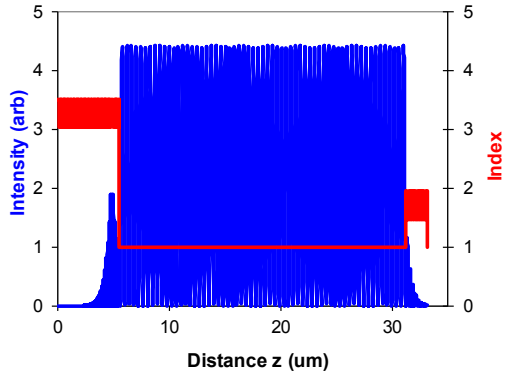

(a)

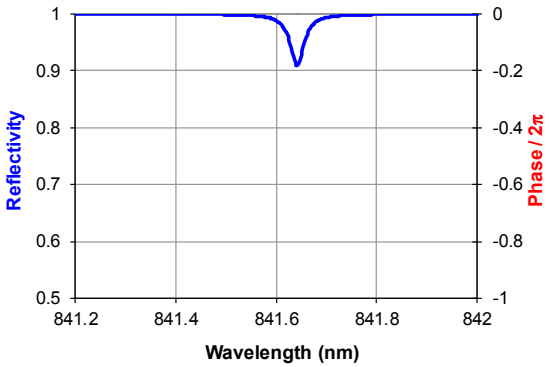

(b)

Figure 7. (a) Optical intensity (blue) at 841.642 nm and index of refraction (red) versus position in the VECSEL cavity. The 841.642-nm mode operates near to resonance on both the semiconductor and external cavities. (b) Zoomed view of the 841.642 nm resonance dip showing a full width at half maximum (FWHM) of 0.0320 nm.

Finally, we consider simulations of the temperature tuning of the five central modes shown in Figure 4. Temperature tuning of wavelength results from increases in length and index of each layer as the temperature is increased. However, the index tuning coefficients dn/dT for GaAs (267 x 10^{-6}/°C) and AlAs (143 x 10^{-6}/°C) strongly dominate wavelength tuning over all other effects, so we only consider semiconductor index tuning effects.[8] Figure 8(a) shows the wavelength tuning versus temperature of the three modes at λ_0 = 850 nm, λ_1 = 841.65 nm, and λ_2 = 829.35 nm. The 850 nm mode tunes relatively quickly versus temperature, at essentially the same rate of 0.06 nm/°C as a standard 850-nm VCSEL. Because the 850-nm mode operates at an anti-resonance of the external cavity, the intensity is peaked in the semiconductor cavity, and the wavelength tuning properties are dominated by the semiconductor index tuning. In contrast, the shorter wavelength modes tune more slowly versus temperature since they operate near resonances of the external cavity and have peak intensity outside of the semiconductor. The numerical temperature tuning coefficients are listed in Figure 8(b). We note that the closer the VECSEL mode is to a resonance of the external cavity, the slower it tunes with changes in the semiconductor indices of refraction.

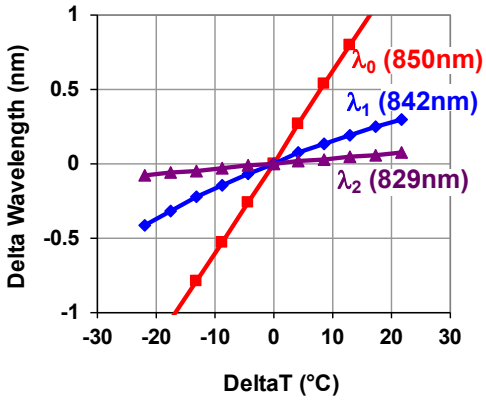

(a)

(b)

Mode	Wavelength (nm)	Tuning (nm/°C)
λ0	850	0.0602
λ1	841.65	0.0161
λ2	829.35	0.0035

Figure 8. (a) Simulated tuning of three VECSEL modes versus temperature. The nominal (un-tuned) wavelengths of these three modes are: $\lambda_0 = 850$nm, $\lambda_1 = 841.65$nm, and $\lambda_2 = 829.35$nm. (b) Temperature tuning coefficients of these three modes.

In summary, we have modeled longitudinal mode selection for single-frequency operation, cold-cavity linewidth that determines the laser linewidth, and temperature tuning of the primary modes of the VECSEL cavity. The following sections will present diagnostic measurements on passive cavities, and measurements of active VECSELs that validate the theoretical predictions of this section.

3. PASSIVE CAVITY MEASUREMENTS

In this section, we discuss spectroscopic measurements of passive laser cavities to determine material properties, such as optical losses. As shown in the modeling section, the resonant modes of the laser cavity manifest as dips in the reflection versus wavelength spectrum. We seek to validate the models by comparing the measured reflection spectra with predictions of the models. Additionally, the losses in the laser cavity can be determined from the widths of the reflection dips. Because un-pumped quantum well gain regions are highly absorbing, we have fabricated diagnostic structures, without quantum well gain regions, to measure only the losses due to other materials in the laser cavity and due to the transmission of the DBR mirrors.

Figure 9(a) shows a schematic diagram of the optical setup used to measure both reflection and transmission versus wavelength. A unique feature of this setup is the ability to measure a laser cavity with lateral optical confinement provided by a curved mirror or an oxide aperture. Because VCSEL and VECSEL cavities have mode diameters in the range of 3 to 20 μm, the input beam is focused to the same diameter to mode match to the laser cavity under test. The setup can be used with either a single-frequency laser input or a broad-band white-light-source input, depending on the wavelength resolution that is required for the measurement. In the case of the white-light-source input, a spectrometer is used to measure the reflection (or transmission) versus wavelength, and the wavelength resolution is in the range 0.02 to 1.00 nm, depending on the length and dispersion of the spectrometer. In the case of a single-frequency laser input, we measure the reflection (or transmission) using a photodiode-based optical power meter while the laser frequency is tuned over a range of wavelengths. The input laser linewidth and tuning accuracy determine the resolution of the spectral measurement, and this method routinely achieves resolutions less than 1 pm.

Figure 10(a) shows the reflection spectrum of a short-cavity VECSEL measured using a white-light-source input and a spectrometer with a resolution of 0.2 nm. The reflection spectrum shows the primary cavity resonance dip at 850 nm, and four satellite longitudinal modes at 824, 840, 859, and 877 nm. The white-light-source probe spot was focused to a diameter of 8 μm to mode-match to the fundamental spatial mode of the plano-concave external cavity. Less pronounced reflection dips that appear in Figure 10(a) are due to higher-order spatial modes. Figure 10(b) shows a schematic drawing of the short-cavity VECSEL device under test.[7] The measured mode spacings indicate that the external-cavity had a free-spectral range of 17 nm, corresponding to an external-cavity length of 21 μm.

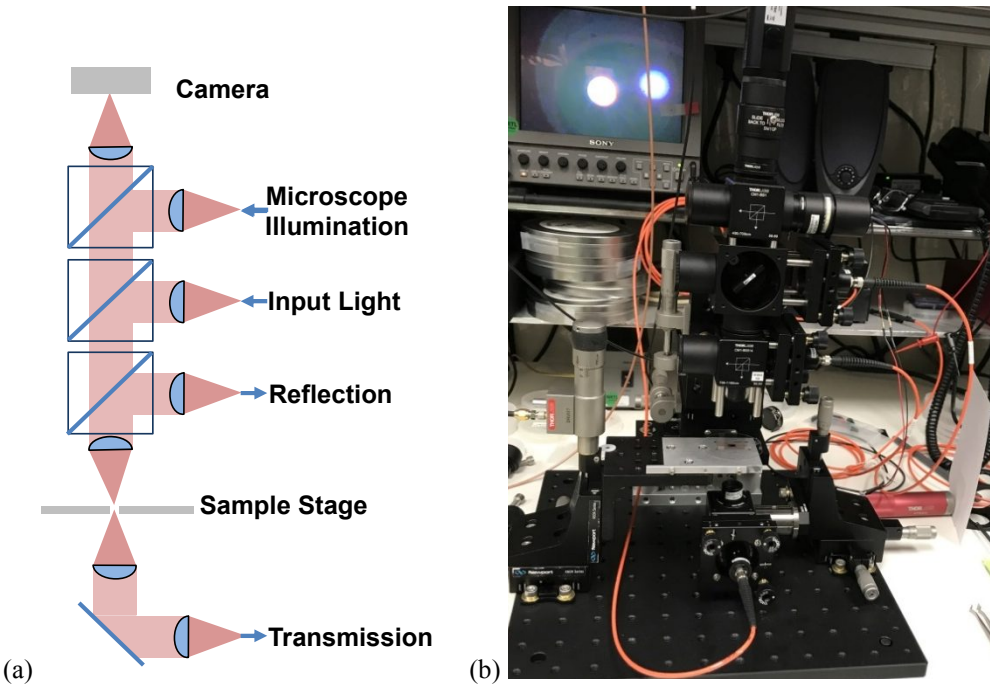

Figure 9. (a) Schematic drawing of the optical reflection/transmission measurement setup. (b) Photograph of the optical reflection/transmission measurement setup showing input and output optical fibers.

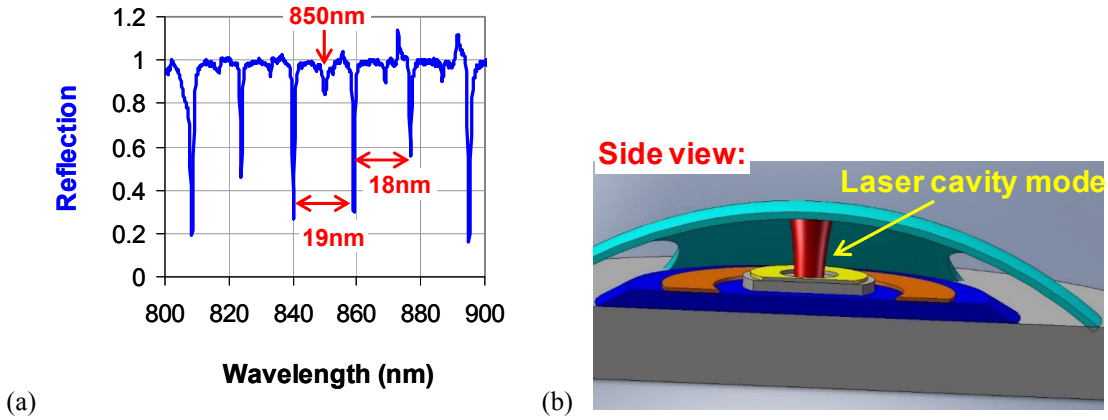

Figure 10. (a) Measured white-light reflection spectrum of a short-cavity VECSEL, showing 5 longitudinal modes between 820 and 880 nm. We deduce from the mode spacings that the external-cavity free-spectral range is 17 nm, corresponding to an external cavity length of 21 μm. (b) Schematic cross-sectional drawing of the short-cavity VECSEL, showing the external cavity between the semiconductor middle DBR (gray) and the external curved mirror (cyan).

Figure 11(a) shows reflection versus wavelength measured on the 800-μm-long external cavity shown in Figure 11(b) that offers a path to further reductions in laser linewidth. We tuned a single-frequency VCSEL across the full 0.24 nm free-spectral range of the external cavity, achieving a wavelength resolution well below 1 pm. A dielectric DBR coating of reflectivity 98.3% was deposited onto the curved side of a plano-convex lens of center thickness 0.8 mm and index 1.85. The same DBR coating was deposited onto a flat BK7 glass window of diameter 12.7 mm. These two optics were joined together with transparent index matching fluid of index 1.7 to create a Fabry-Perot cavity of length 0.8 mm and index 1.85. The measured free-spectral range (FSR) of 0.24 nm at a wavelength of 850 nm is consistent with the known cavity length and index of refraction. The inset in Figure 11(a) shows the measured cold-cavity linewidth of 1.3 pm (0.54 GHz) that determines a round-trip power loss of 3.4%, suggesting that less than 0.1% excess cavity loss resulted

from the net effects of absorption, scattering, and surface form errors. Measuring cavity finesse (or quality factor) is the best way to accurately determine optical losses (due to transmission, absorption, scattering, etc.) as they will manifest in a real VECSEL cavity.

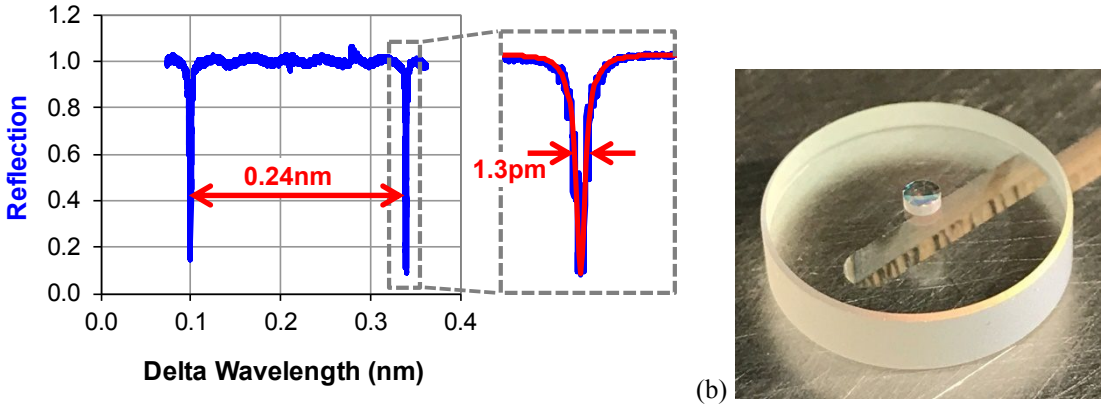

Figure 11. (a) Reflection versus wavelength resolving the linewidth of a cavity mode to determine the round-trip loss in the cavity. (b) A 0.8-mm-long glass cavity using two dielectric reflectors of reflectivity R = 98.3%.

4. ACTIVE VECSEL MEASUREMENTS

We fabricated a released dielectric DBR dome over a VCSEL base structure, as reported previously,[7] yielding the VECSEL device shown in Figure 12(a). The photograph shows the VECSEL lasing with an input drive current of 4 mA. The implant aperture diameter is 10 µm. Optical power and voltage data versus current for this same device are shown in Figure 12(b). The threshold current was 2.3 mA and the output power was 2.8 mW at a drive current of 6 mA. The series resistance of this device was high (500 Ω), which was due to spreading resistance into the implant aperture within the low-mobility p-type middle DBR layers. The VECSEL achieved a high differential quantum efficiency of 60%, which indicates low optical losses in the cavity relative to output coupling.

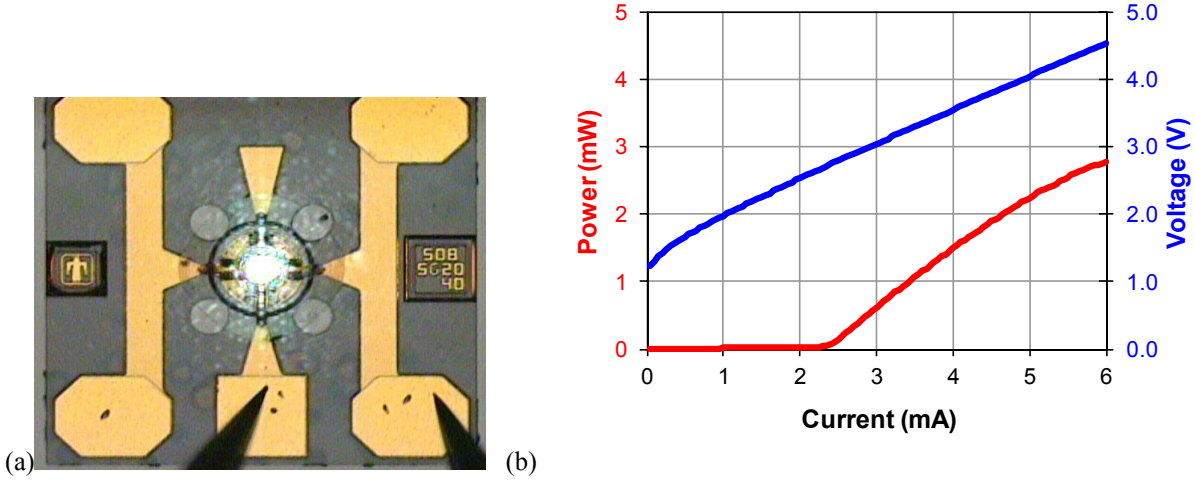

Figure 12. (a) Microscope photograph of an electrically-pumped VECSEL with an external cavity length of 25 microns. (b) VECSEL output optical power and voltage drop versus current, exhibiting a 2.3 mA threshold current and 2.8 mW output power at 6 mA drive current.

Single-frequency emission was observed over the full range of operating currents, as shown by the optical spectrum in Figure 13(a) that exhibits a side-mode suppression ratio exceeding 40 dB. Operation in a single-transverse mode was anticipated, largely based on the matched spatial overlap of the implant gain aperture with the fundamental Gaussian optical mode of the external cavity. As described in the modeling section, the 25-µm-long external cavity should

produce longitudinal modes at wavelengths 8 nm shorter and longer than the primary VECSEL mode. Figure 13(a) shows that any emission into these satellite longitudinal modes was suppressed by least 50 dB relative to the primary laser emission. Measurements of emission spectra from several VECSEL devices on this wafer confirmed our theoretical prediction of single longitudinal mode operation, due to the 8-fold increase in predicted threshold gain for the two satellite longitudinal modes relative to the central laser mode. Figure 13(b) shows the measured wavelength tuning versus temperature of the VECSEL, indicating a temperature tuning coefficient of 0.046 nm/°C, similar to that of a standard VCSEL. The measured temperature tuning coefficient is consistent with the model predictions from section 2 for the central (850 nm) mode of the VECSEL. In addition, mode hopping was not observed across the measured temperature tuning range.

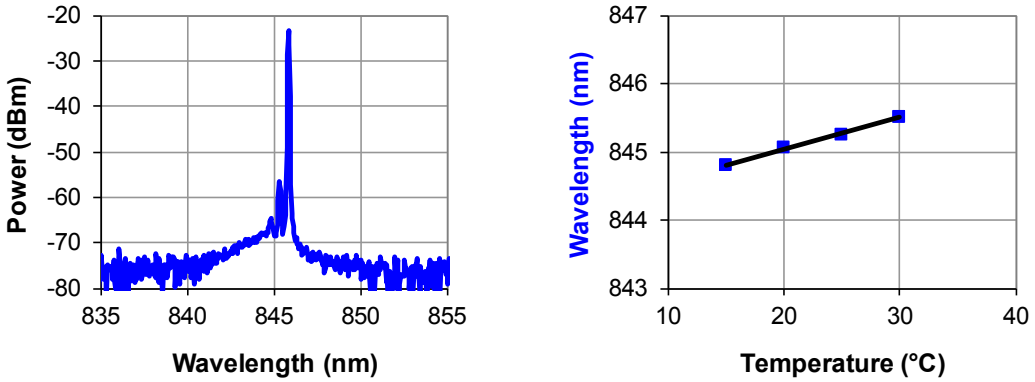

(a) (b)

Figure 13. (a) Single mode emission spectrum of the VECSEL, measured at a drive current of 4 mA. (b) Plot of wavelength versus temperature showing a temperature tuning rate of 0.046 nm/°C for the lasing VECSEL.

Figure 14(a) shows a schematic diagram of the optical heterodyne measurement setup that we employed to measure the linewidth of the 846-nm VECSEL described above.[9] For this measurement, an external-cavity diode laser (linewidth < 1 MHz) at 846-nm was tuned to a frequency f_1, approximately 0.28 GHz below the VECSEL frequency f_2. The two optical beams were combined using a 50% beam splitter and coupled into an 850-nm single-mode fiber and detected with a 12-GHz photoreceiver (New Focus model 1580-B) whose output was fed into an electrical spectrum analyzer.

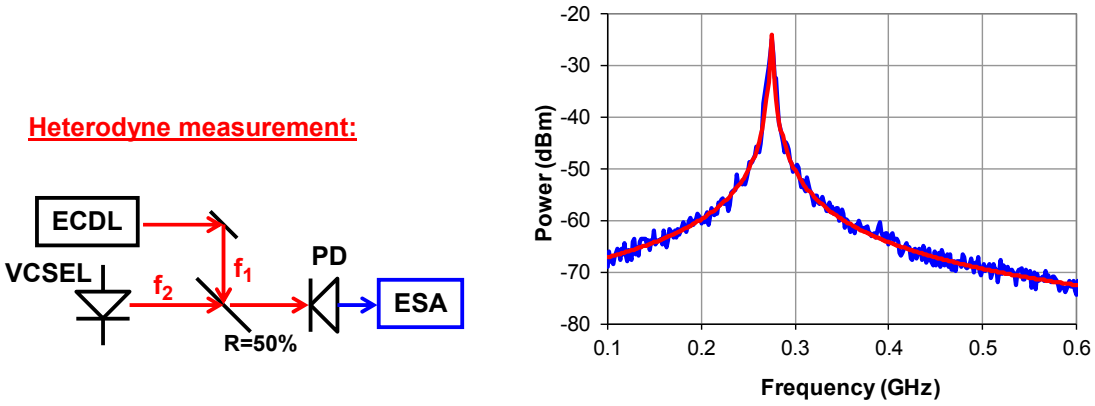

(a) (b)

Figure 14. (a) Schematic of the heterodyne linewidth measurement setup, showing an external-cavity diode laser (ECDL), a photodiode (PD), and an electrical spectrum analyzer (ESA). (b) Heterodyne linewidth measurement of the VECSEL exhibiting a 2 MHz linewidth.

The spectrum analyzer resolution bandwidth was set to 0.3 MHz. The resulting beat note appeared at approximately 0.28 GHz, as shown in Figure 14(b). A Lorentzian with a 2-MHz FWHM linewidth fits the data well. The VECSEL drive current for this measurement was 5 mA, which was supplied by a low-noise current source. Also, the VECSEL was temperature stabilized in an oven to minimize thermal frequency drifts during the measurement. Based on the

narrowing of the cold-cavity linewidth relative to a standard VCSEL, we would expect the VECSEL linewidth to be below 1 MHz. However, due to the large temperature tuning coefficient, it is difficult to stabilize temperature and drive current sufficiently to measure a 1 MHz VECSEL linewidth during the 420 ms sweep time of the spectrum analyzer.

5. CONCLUSIONS

In summary, we have considered the design and performance of three-mirror coupled-cavity VECSELs for next-generation low-power atomic clocks. Desired VECSEL characteristics for these applications are (1) single-frequency operation, (2) narrow laser linewidth (ideally less than 1 MHz), and (3) temperature tuning of wavelength without mode hops. We simplified the three-mirror VECSEL model to an equivalent two-mirror laser model, treating the external-cavity section as a single (Fabry-Perot) effective mirror that has highest reflectivity at anti-resonances and lower reflectivity (and rapid phase shift) at resonances. We solved the equivalent two-mirror laser model for a specific VECSEL design that we have fabricated and characterized. The model revealed a dominant low-threshold mode with a narrow cold-cavity linewidth, consistent with the goals of single-frequency operation and narrow laser linewidth. Moreover, the model showed that the dominant laser mode tunes with temperature at nearly the same rate as a regular VCSEL. We presented VECSEL measurements showing single-frequency operation, wavelength tuning versus temperature, and a 2 MHz linewidth. All of the measured VECSEL characteristics are consistent with the predictions of the model. The theoretical model of the three-mirror coupled-cavity VECSEL that we presented also provides design intuition for rapidly evaluating alternative VECSEL cavity designs.

ACKNOWLEDGMENTS

The authors wish to thank V. M. Sanchez and T. M. Bauer for their expert technical assistance. We also thank R. Lutwak for asking the stimulating questions that inspired this paper. This material is based in part upon work supported by the Defense Advanced Research Projects Agency (DARPA) under Contract No. HR0011730802. The views, opinions and/or findings expressed are those of the author and should not be interpreted as representing the official views or policies of the Department of Defense or the U.S. Government. Sandia National Laboratories is a multimission laboratory managed and operated by National Technology and Engineering Solutions of Sandia, LLC., a wholly owned subsidiary of Honeywell International, Inc., for the U.S. Department of Energy's National Nuclear Security Administration under contract DE-NA-0003525.

REFERENCES

[1] J. Kitching, S. Knappe, N. Vukicevic, L. Hollberg, R. Wynands, and W. Weidmann, "A Microwave Frequency Reference Based on VCSEL-Driven Dark Line Resonances in Cs Vapor," IEEE Trans. Instrum. Meas. 49, pp. 1313–1317 (2000).

[2] R. Lutwak, A. Rashed, M. Varghese, G. Tepolt, J. Leblanc, M. Mescher, D. K. Serkland, and G. M. Peake, "The miniature atomic clock - Pre-production results", Proceedings of the 2007 IEEE International Frequency Control Symposium, Geneva, Switzerland, pp. 1327-1333 (2007).

[3] S. Jefferts, J. Shirley, T. Parker, T. Heavner, D. Meekhof, C. Nelson, F. Levi, G. Costanzo, A. DeMarchi, R. Drullinger, L. Hollberg, W. Lee, F. Walls, "Accuracy evaluation of NIST-F1," Metrologia 39, p. 321 (2002).

[4] A. L. Schawlow, and C. H Townes, "Infrared and Optical Masers," Physical Review 112, pp. 1940-1949 (1958).

[5] C. H. Henry, "Theory of the linewidth of semiconductor lasers," IEEE J. Quantum Electronics QE-18, pp. 259-264 (1982).

[6] L. A. Coldren, S. W. Corzine, M. L. Masonovic, *Diode Lasers and Photonic Integrated Circuits, second edition*, Wiley, Hoboken, New Jersey, Chapter 3 (2012).

[7] D. K. Serkland, K. M. Geib, G. A. Keeler, G. M. Peake, "Fully micro-fabricated VECSEL at 850 nm," Proceedings of the SPIE, vol. 7952, pp. 79520L (2011).

[8] J. Talghader, and J. S. Smith, "Thermal dependence of the refractive index of GaAs and AlAs measured using semiconductor multilayer optical cavities," Appl. Phys. Lett. 66, pp. 335-337 (1995).

[9] D. K. Serkland, G. A. Keeler, K. M. Geib, and G. M. Peake, "Narrow Linewidth VCSELs for High-Resolution Spectroscopy," Proc. SPIE, vol. 7229, article 722907 (2009).